GEOPHYSICAL RESEARCH LETTERS, VOL. 33, L03608, doi:10.1029/2005GL025084, 2006

Wind-driven zonal jets in the South Pacific Ocean

William S. Kessler[1] and Lionel Gourdeau[2]

Received 28 October 2005; revised 22 December 2005; accepted 4 January 2006; published 10 February 2006.

[1] Zonal jets west of the large islands of the South Pacific Ocean are predicted by theory, commonly seen in ocean models with sufficiently high resolution, and are beginning to be observed. These jets are often taken to reflect the blocking effect of the islands in the South Equatorial Current through "Island Rule" dynamics. Here it is shown that quasi-permanent structures of the basin-wide wind field imply the existence of jets formed independently of the islands. Evidence for the existence of the wind-driven jets is found in climatological geostrophic currents. The hydrographic structures that produce the jets occur well below the thermocline. **Citation:** Kessler, W. S., and L. Gourdeau (2006), Wind-driven zonal jets in the South Pacific Ocean, *Geophys. Res. Lett.*, *33*, L03608, doi:10.1029/2005GL025084.

1. Introduction

[2] In recent years, high-spatial-resolution ocean model simulations of the circulation of the South Pacific have suggested the presence of narrow zonal jets extending west of the northern and southern tips of the large island groups (Fiji, Vanuatu and New Caledonia) that obstruct the South Equatorial Current (SEC) [*Webb*, 2000]. Analyses of hydrographic data confirm the presence of zonal jets in the Coral Sea [*Sokolov and Rintoul*, 2000; *Qu and Lindstrom*, 2002; *Ridgway and Dunn*, 2003]. Similar features have been observed west of the Hawaiian Island chain [*Qiu and Durland*, 2002] and south of Fiji [*Stanton et al.*, 2001]. The occurrence of such jets is expected under the extension of Sverdrup theory to include the effects of blocking islands [*Godfrey*, 1989], and it has been assumed that the west Pacific jets are due to the islands. The purpose of the present work, however, is to document quasi-permanent meridional structure in the basin-wide Pacific wind field that generates jets in the SEC well east of the islands.

2. Data

[3] The principal wind data set used here to characterize the Sverdrup circulation is from the European Remote Sensing (ERS) satellite scatterometer, which was launched in 1991, and including a follow-on mission, remained in operation through 2000. The ERS scatterometer samples a swath 500 km wide with an effective along-track resolution of 50 km [*Stoffelen and Anderson*, 1997]. The winds used here were processed into monthly, 1° latitude by 1° longitude gridded fields of stress components by the Centre ERS d'Archivage et de Traitement (CERSAT) and obtained from their web site (http://www.ifremer.fr/cersat). A monthly average annual cycle was constructed from the 9.5 years of data, and the mean of that cycle was used for the curl and Sverdrup transports.

[4] Data from the QuikSCAT satellite carrying a SeaWinds scatterometer (referred to here as QuikSCAT), launched in mid-1999 and remaining in operation, were used to supplement the ERS winds. The QuikSCAT swath is 1600 km wide with an effective resolution of less than 10 km [*Schlax et al.*, 2001]. The version used here was processed into monthly 1/2° by 1/2° bins by CERSAT, and obtained from the same website as the ERS winds.

[5] Temperature and salinity fields compiled and objectively analyzed by *Levitus et al.* [1994] and *Levitus and Boyer* [1994] were used to describe the ocean vertical structure and geostrophic currents in the east-central Pacific.

[6] Mean absolute surface dynamic topography was obtained by subtracting the geoid based on the GRACE satellite gravity mission from the 1993–1999 mean altimetric sea surface height from the TOPEX/Poseidon satellite altimeter [*Gourdeau et al.*, 2003]. The geoid was the EIGEN-GRACE02S Earth gravity field model developed to degree 60 [*Reigber et al.*, 2004]; and the mean sea surface is the CLS01 solution [*Hernandez and Schaeffer*, 2001]. The formal cumulative error of the mean dynamic topography is as large as 4 cm.

3. Results

[7] The wind stress curl field in the South Pacific (Figure 1a) is comparable to that of the other subtropical gyres, with anticyclonic curl in the subtropics, and cyclonic curl in the deep tropics. The pattern is complicated by the South Pacific Convergence Zone (SPCZ), which extends from New Guinea to about 15°S, 150°W, identified by a zero curl line with negative values to its south in Figure 1a, while the southeast trades continue to the equator in the east. The trade wind maximum is marked by a zero curl line along 20°S in the west and 5°–15°S in the east.

[8] Under Sverdrup dynamics (ignoring islands), the predicted meridional transport is $V_{Sv} = Curl(\tau)/(\beta\rho)$, and the zonal transport is found from continuity, integrating the meridional divergence westward from the eastern boundary:

$$U_{Sv} = -\int_{EB}^{x} \frac{\partial V}{\partial y}\, dx' = -\frac{1}{\beta\rho}\int_{EB}^{x} \frac{\partial [Curl(\tau)]}{\partial y}\, dx' \qquad (1)$$

(Since the integration is westward, dx' is taken to be negative). The overall picture is of westward flow (the SEC) due to the large-scale trend from positive to negative curl,

[1]NOAA/Pacific Marine Environmental Laboratory, Seattle, Washington, USA.
[2]Institut de Recherche pour le Développement, Nouméa, New Caledonia.

0094-8276/06/2005GL025084$05.00

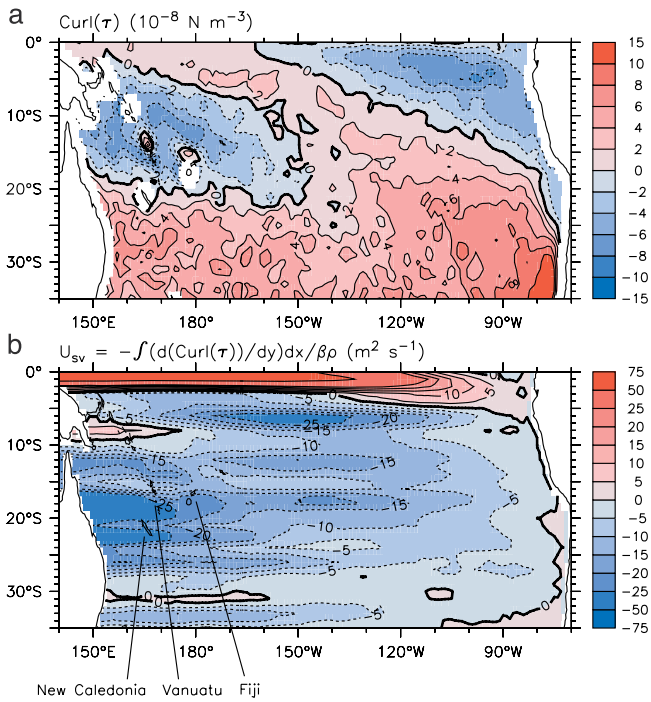

Figure 1. (a) Mean Curl(τ) (10^{-8} N m^{-3}) from ERS winds over 1991–2000. (b) Zonal Sverdrup transport (m^2 s^{-1}) calculated from the ERS curl using (1). The three large island groups of the southwest Pacific are indicated in the bottom panel, however, the calculation of the Sverdrup transport assumed that the islands were absent (the curl was linearly interpolated across the gaps).

but the details of Curl(τ) produce significant structure in the Sverdrup currents. The zonal transport derived from the ERS winds using (1) shows the SEC broken into jets in mid-basin, with minima at 10°S, 15°S, 24°S and 30°S (Figure 1b). These jets weaken somewhat along the south flank of the SPCZ, where the curl gradient changes sign, but they restrengthen under the trade wind maximum near the dateline, with additional jets formed to the south, still east of the major islands. Note that three of these occur at the latitudes where *Webb* [2000] identified jets due to islands (at 13°S, passing north of Vanuatu, at 18°S north of New Caledonia, and at 23°S south of New Caledonia), however, the Sverdrup jets in Figure 1b are generated entirely by the winds, and occur thousands of km east of these islands.

[9] In addition to blocking ocean currents, the occurrence of a high island also disrupts the low-level winds, leading to dipoles of positive and negative curl downwind of the island, which can have a substantial impact on the ocean [*Xie et al.*, 2001; *Chavanne et al.*, 2002; *Chelton et al.*, 2004]. Such dipoles are visible downwind of Fiji and Vanuatu, and weakly behind New Caledonia (Figure 1a). The resulting curl gradient between the dipoles west of these islands is an eastward tendency in (1). The effect of these island-induced curl features contributes to the zonal transport minima west of these islands (Figure 1b); probably coincidentally, these occur close to the latitudes where the minima between the mid-basin jets already existed, and thereby reinforce the jetlike tendency.

[10] Since the zonal transport depends on the second derivative of the winds, the features of the windfield that produce this meridional structure are not apparent in the windfield itself, which varies smoothly across the entire subtropics in mid-basin where the Sverdrup jets arise (Figure 2). Even the curl is relatively smooth (and note that the curl at these longitudes is almost entirely due to the zonal wind variation). Nevertheless, the second derivative term inside the integral on the right side of (1) has substantial meridional structure that produces the Sverdrup jets.

[11] An obvious question is whether the mean wind pattern shown in Figure 2 is in fact a good representation of a long-term mean, or might be simply the aliasing of a transient event in the relatively short scatterometer wind record. Certainly the very strong anomalies associated with the 1997–98 El Niño have the potential to contaminate this average. To examine this possibility, Figure 3 shows a time series of the curl derivative term inside the integral (1), in the 150°W–110°W region where the integral grows westward. Blue shading (dashed contours) shows negative values, which will enhance westward flow in (1). The ERS time series has been extended by adding Quikscat winds through 2004 (note that no blending of these winds was done, and Figure 3 is simply two independent plots aligned side-by-side). While the Quikscat winds show additional detail at smaller scales, the continuity of the two time series is clear. Throughout these records, the tendency toward positive (or weaker negative) values of the curl derivative at about 10°S, 15°S, and 23°S is seen. The features in the winds that produce the Sverdrup zonal jets are not just an aliasing of one or a few large anomalous events, but appear to be quasi-permanent, at least during the past 13 years.

[12] Although the hydrographic data record is quite sparse in the South Pacific, geostrophic transports relative to 2000 m from the *Levitus and Boyer* [1994] climatology show westward minima at 9°S and 15°S in mid-basin, in relatively good agreement with the Sverdrup prediction

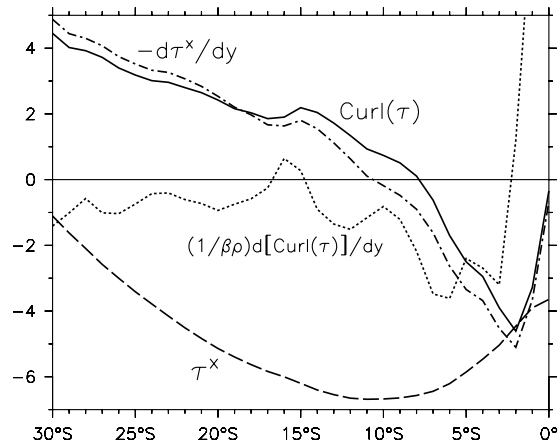

Figure 2. Meridional structure of the wind and its derivatives at 150°W–110°W, the longitude range over which the integral (1) grows fastest. Zonal wind stress (τ^x) (dashed, 10^{-2} N m^{-2}), Curl(τ) (solid, 10^{-8} N m^{-3}), $-d\tau^x/dy$ (dash-dot, 10^{-8} N m^{-3}), $(1/\beta\rho)$d[Curl(τ)]/dy (dotted, 10^{-6} m s^{-1}).

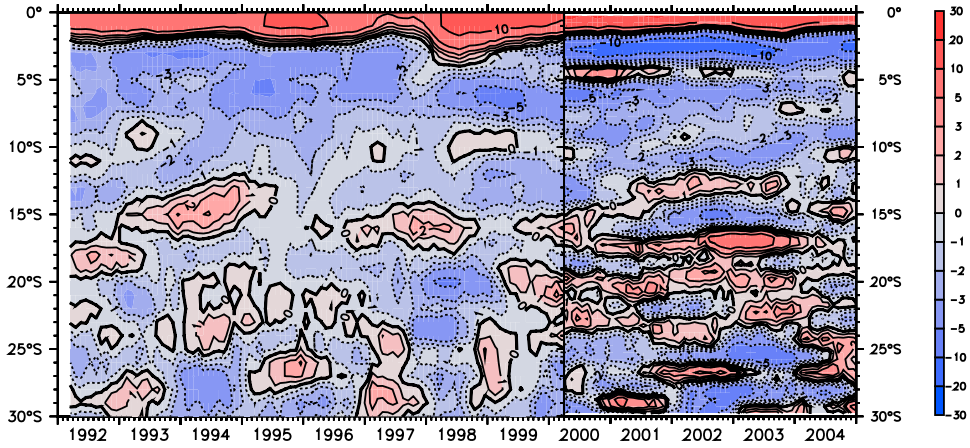

Figure 3. One-year running mean time series of $(1/\beta\rho)\partial[\mathrm{Curl}(\tau)]/\partial y$ (term inside the integral (1)) (10^{-6} m s^{-1}), averaged over 150°W–110°W. Negative values (blue; dashed contours) produce a westward tendency, positive (red; solid contours) eastward. ERS winds are shown before April 2000, and QuikSCAT winds thereafter. No blending of the winds was done; the two plot panels are independent. For the QuikSCAT winds, which have finer detail than ERS, the region immediately adjacent to the Marquesas Islands (7.5°S–11°S, 145°W–141°W) is omitted from the average to avoid the very large curl due to wind funneling around the high mountains of the islands.

(Figure 4). However, the predicted structures between 18°S and 24°S are only weakly seen in this data set. Surface absolute zonal geostrophic currents estimated from geoid-referenced satellite altimetry also mirror the pattern of minima and maxima in the Sverdrup SEC (Figure 4).

[13] *Reid* [1986] noted that the South Pacific subtropical gyre extends deeper than those of the other basins; consistent with this, the jet-like structures seen in Figure 4 are not fully apparent until the dynamic height integration is carried to 2000 m. In the Levitus climatology, zonal geostrophic currents east of the major islands show a relatively smooth SEC in the tropical thermocline, deepening below the near-surface eastward Subtropical Countercurrent (STCC) south of 20°S (Figure 5). The STCC is due to the upward turn of isopycnals peeling off toward the surface above the thermocline, while the bowl of the gyre occurs further south with increasing density. Below the SEC, the upward bulge of isopycnals deeper than $\sigma_\theta = 26$ tilts southward with depth in a similar pattern, with the shallowest point of 26 near 3°S, of 27 near 11°S, of 27.25 near 15°S, and of 27.5 near 18°S (Figure 5). As a result, eastward flow maxima occur near 3°S at 250 m depth (the southern Tsuchiya Jet [*Rowe et al.*, 2000]), at 10°S at 500 m depth, and at 15°S at about 1000 m depth, and these produce most of the minima that disrupt the vertically-integrated SEC seen in Figure 4.

4. Conclusion

[14] While there is no doubt that the large island groups of the western tropical Pacific interrupt the SEC and produce narrow "Island Rule" westward jets at their tips, that appears to be only part of the explanation for the South Pacific jets. Detailed structure of the mid-Pacific winds breaks the SEC into several bands of stronger flow as far east as 120°W, according to linear Sverdrup dynamics where the islands are ignored (Figure 1). The west Pacific jets are therefore due to three processes acting in sequence: mid-basin bands of stronger flow are created by the wind, then curl dipoles behind the high islands intensify the minima behind the islands, and blocking of the ocean currents by the islands further narrows the jets. It is probably a coincidence that the mid-basin wind structure is such as to initiate jets close to the latitudes between the large west Pacific islands so the three effects reinforce each other.

[15] The reason for the seemingly-minor meridional variability of the mid-basin winds (Figure 2) remains unknown. Since the Sverdrup jets arise well east of all the high islands that might modify the winds, it probably is not attributable to surface effects. Although this pattern appears to have preferred locations over the 13 years of scatterometer wind records (Figure 3), there is substantial time variability. The possibility should also be considered that the wind structure might be an artifact of the satellite

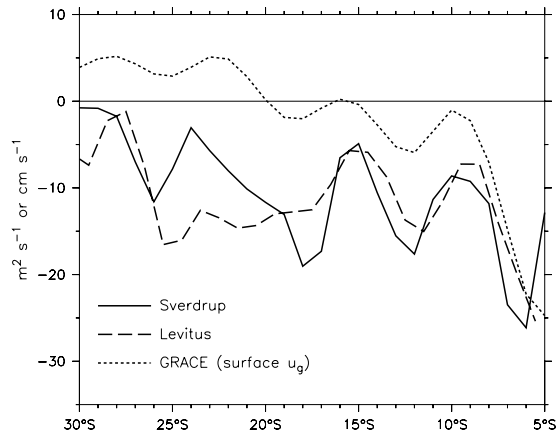

Figure 4. Zonal transport/width (m^2 s^{-1}) averaged over 160°W to 130°W from the Sverdrup relation (1) (solid), and from the Levitus ocean climatology (dashed). Absolute surface zonal geostrophic current (cm s^{-1}), from 1993–1999 mean Topex/Poseidon altimetric sea surface height referenced to the GRACE geoid (dotted).

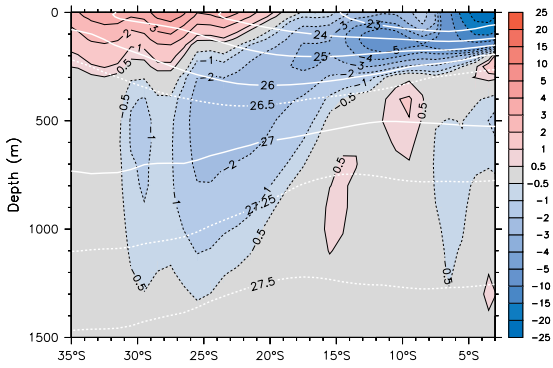

Figure 5. Zonal geostrophic current relative to 2000 m (cm s^{-1}) (color shading), with overlaid (white) contours of density (σ_θ), averaged over 160°W–130°W, from the Levitus climatology. Density contours are every kg m^{-3}, with supplementary dashed contours at 26.5, 27.25, and 27.5.

scatterometer data processing algorithms, which must account for partly-sampled atmospheric contamination of the signal by water vapor, or by rain effects [*Chelton and Freilich*, 2005]. However, the fact that the wind variations seem to be fairly accurately imprinted on the independently-observed ocean currents (Figure 4) suggests that this is a real phenomenon.

[16] A further unknown is the adjustment process by which the ocean responds to this element of forcing by producing eastward currents at great depth (Figure 5), well below the thermocline that would be expected to feel the wind variations most straightforwardly. The fact that the bulge of isotherms that result in the deep eastward currents below the SEC appears to begin with the southern Tsuchiya jet at about 3°S near 250 m depth [*Rowe et al.*, 2000] may be a clue that the dynamics originate in upwelling along the coast of South America, whose effects propagate into the subthermocline mid-basin along curved Rossby wave ray characteristics [*Luyten et al.*, 1983; *McCreary et al.*, 2002].

[17] **Acknowledgments.** We thank J. M. Lemoine for providing the satellite mean dynamic topography. Contribution 2876 from the Pacific Marine Environmental Laboratory.

References

Chavanne, C., P. Flament, R. Lumpkin, B. Dousset, and A. Bentamy (2002), Scatterometer observations of wind variations induced by oceanic islands: Implications for wind-driven ocean circulation, *Can. J. Remote Sens.*, *28*(3), 466–474.

Chelton, D. B., and M. H. Freilich (2005), Scatterometer-based assessment of 10-m wind analyses from the operational ECMWF and NCEP numerical weather prediction models, *Mon. Weather Rev.*, *133*(2), 409–429.

Chelton, D. B., M. G. Schlax, M. H. Freilich, and R. F. Milliff (2004), Satellite radar measurements reveal short-scale features in the wind stress field over the world ocean, *Science*, *303*, 978–983.

Godfrey, J. S. (1989), A Sverdrup model of the depth-integrated flow for the world ocean allowing for island circulations, *Geophys. Astrophys. Fluid Dyn.*, *45*(1–2), 89–112.

Gourdeau, L., J. M. Lemoine, M. H. Rio, and F. Hernandez (2003), Estimating mean dynamic topography in the tropical Pacific Ocean from gravity and altimetry satellites, *Geophys. Res. Lett.*, *30*(20), 2062, doi:10.1029/2003GL018200.

Hernandez, F., and P. Schaeffer (2001), The CLS01 Mean Sea Surface: A validation with the GSFC00.1 surface, report, 14 pp., CLS, Ramonville St Agne, France.

Levitus, S., and T. Boyer (1994), *World Ocean Atlas 1994*, vol. 4, *Temperature*, *NOAA Atlas NESDIS 4*, NOAA, Silver Spring, Md.

Levitus, S., R. Burgett, and T. Boyer (1994), *World Ocean Atlas 1994*, vol. 3, *Salinity*, *NOAA Atlas NESDIS 3*, NOAA, Silver Spring, Md.

Luyten, J. R., J. Pedlosky, and H. Stommel (1983), The ventilated thermocline, *J. Phys. Oceanogr.*, *13*, 292–309.

McCreary, J. P., P. Lu, and Z. Yu (2002), Dynamics of the Pacific subsurface countercurrents, *J. Phys. Oceanogr.*, *32*, 2379–2404.

Qiu, B., and T. S. Durland (2002), Interaction between an island and the ventilated thermocline: Implications for the Hawaiian Lee Countercurrent, *J. Phys. Oceanogr.*, *32*(12), 3408–3426.

Qu, T., and E. J. Lindstrom (2002), A climatological interpretation of the circulation in the western South Pacific, *J. Phys. Oceanogr.*, *32*, 2492–2508.

Reid, J. L. (1986), On the total geostrophic circulation of the South Pacific Ocean: Flow patterns, tracers and transports, *Prog. Oceanogr.*, *16*, 1–61.

Reigber, C., R. Schmidt, F. Flechtner, R. Konig, U. Meyer, K.-H. Neumayer, P. Schwintzer, and S. Y. Zhu (2004), An earth gravity field model complete to degree and order 150 from GRACE: EIGEN-GRACE02S, *J. Geodyn.*, *39*, 1–10.

Ridgway, K. R., and J. R. Dunn (2003), Mesoscale structure of the mean East Australia Current System and its relation with topography, *Prog. Oceanogr.*, *56*, 189–222.

Rowe, G. D., E. Firing, and G. C. Johnson (2000), Pacific equatorial subsurface countercurrent velocity, transport and potential vorticity, *J. Phys. Oceanogr.*, *30*, 1172–1187.

Schlax, M. G., D. B. Chelton, and M. H. Freilich (2001), Sampling errors in wind fields constructed from single and tandem scatterometer datasets, *J. Atmos. Oceanic Technol.*, *18*, 1014–1036.

Sokolov, S., and S. Rintoul (2000), Circulation and water masses of the southwest Pacific: WOCE section P11, Papua New Guinea to Tasmania, *J. Mar. Res.*, *58*, 223–268.

Stanton, B., D. Roemmich, and M. Kosro (2001), A shallow zonal jet south of Fiji, *J. Phys. Oceanogr.*, *31*(10), 3127–3130.

Stoffelen, A., and D. L. T. Anderson (1997), Scatterometer data interpretation: Estimation and validation of the transfer function CMOD4, *J. Geophys. Res.*, *102*(C3), 5767–5780.

Webb, D. J. (2000), Evidence for shallow zonal jets in the South Equatorial Current region of the Southwest Pacific, *J. Phys. Oceanogr.*, *30*, 706–720.

Xie, S. P., W. T. Liu, Q. Liu, and M. Nonaka (2001), Far-reaching effects of the Hawaiian Islands on the Pacific ocean-atmosphere system, *Science*, *292*, 2057–2060.

L. Gourdeau, Institut de Recherche pour le Développement, Nouméa, New Caledonia. (lionel.gourdeau@noumea.ird.nc)

W. S. Kessler, NOAA/Pacific Marine Environmental Laboratory, Seattle, WA 98115, USA. (william.s.kessler@noaa.gov)